

RESEARCH ARTICLE

Open Access



Identification of the targets of hematoporphyrin derivative in lung adenocarcinoma using integrated network analysis

Hongtao Yin¹ and Yan Yu^{2*}

Abstract

Background: Hematoporphyrin derivative (HPD) has a sensibilization effect in lung adenocarcinoma. This study was conducted to identify the target genes of HPD in lung adenocarcinoma.

Methods: RNA sequencing was performed using the lung adenocarcinoma cell line A549 after no treatment or treatment with X-ray or X-ray + HPD. The differentially expressed genes (DEGs) were screened using Mfuzz package by noise-robust soft clustering analysis. Enrichment analysis was carried out using “BioCloud” online tool. Protein–protein interaction (PPI) network and module analyses were performed using Cytoscape software. Using WebGestalt tool and integrated transcription factor platform (ITFP), microRNA target and transcription factor (TF) target pairs were separately predicted. An integrated regulatory network was visualized with Cytoscape software.

Results: A total of 815 DEGs in the gene set G1 (continuously dysregulated genes along with changes in processing conditions [untreated—treated with X-ray—X-ray + treated with HPD]) and 464 DEGs in the gene set G2 (significantly dysregulated between X-ray + HPD-treated group and untreated/X-ray-treated group) were screened. The significant module identified from the PPI network for gene set G1 showed that ribosomal protein L3 (*RPL3*) gene could interact with heat shock protein 90 kDa alpha, class A member 1 (*HSP90AA1*). TFs AAA domain containing 2 (*ATAD2*) and protein inhibitor of activated STAT 1 (*PIAS1*) were separately predicted for the genes in gene set G1 and G2, respectively. In the integrated network for gene set G2, ubiquitin-specific peptidase 25 (*USP25*) was targeted by *miR-200b*, *miR-200c*, and *miR-429*.

Conclusion: *RPL3*, *HSP90AA1*, *ATAD2*, and *PIAS1* as well as *USP25*, which is targeted by *miR-200b*, *miR-200c*, and *miR-429*, may be the potential targets of HPD in lung adenocarcinoma.

Keywords: Lung adenocarcinoma, Hematoporphyrin derivative, X-ray, Protein–protein interaction network, Integrated network

Background

Lung/pulmonary adenocarcinoma, a common type of lung cancer, possesses some malignant characteristics such as duct formation, gland formation, and excessive production of mucus [1]. Although smoking is

responsible for most lung adenocarcinoma cases, lung adenocarcinoma is also very common in passive smokers or people with irregular smoking habit [2, 3]. In the United States, approximately 40% cases of lung cancer are lung adenocarcinoma, which often originates from the peripheral lung tissue [4] probably because the filters in cigarettes prevent the entry of the bulky grains into the lungs [5]. Although adenocarcinoma produces smaller masses and develops slowly as compared with the other

*Correspondence: Yuuny_HTH@hotmail.com

² Department of Medical Oncology, Harbin Medical University Cancer Hospital, No. 150 Haping Road, Nangang District, Harbin 150081, Heilongjiang, China

Full list of author information is available at the end of the article



types of lung cancers, it is likely to show distant metastasis at an early stage [6]. Therefore, evaluation of the mechanisms underlying lung adenocarcinoma progression is desirable to improve treatment outcomes.

Porphyrins may selective accumulate in malignant tumors [7], and hematoporphyrin derivative (HPD) has been used as a photosensitizer in the photodynamic therapy (PDT) of lung cancer [8]. It was demonstrated that 99mTc-hematoporphyrin-linked albumin nanoparticles (99mTc-HP-ANPs) may be used for the PDT and radio-diagnosis of lung cancer [9]. The combination of PDT and photosensitizers HPD and 5-aminolevulinic acid (ALA) may increase the curative rate for skin cancers, distinctly cut down the photosensitive period, and reduce the dose of pro-toxic HPD [10]. Hematoporphyrin conjugated with the antibodies directed to vascular endothelial growth factor shows high antitumor activities in patients with Lewis lung carcinoma [11]. The expression level of interleukin-6 affects the cellular sensitivity to PDT, and the combination of PDT and interleukin-6 may serve as a novel strategy for the therapy of Lewis lung carcinoma [12]. Wang et al. used X-ray as the energy source for PDT activation and suggested that the X-ray-induced photodynamic therapy (X-PDT) may be used as a novel therapeutic method against human cancers [13]. Austerlitz et al. found that the response of the Fricke solution doped with hematoporphyrin and irradiated with low-energy X-rays was enhanced in PDT [14]. However, the mechanism underlying HPD effects in lung adenocarcinoma are not investigated.

As a commonly studied lung adenocarcinoma cell line, A549 was used as a model in the present study. RNA

sequencing was applied to the untreated A549 cells as well as those treated with X-ray or the combination of X-ray and HPD. The differentially expressed genes (DEGs) were screened and enrichment analysis, protein-protein interaction (PPI) network, and module analyses as well as integrated network analysis were carried out to identify the important genes affected by HPD.

Materials and methods

Cell cultivation

The lung adenocarcinoma cell line A549 was acquired from the Cell Bank of Chinese Academy of Sciences. The cells were cultured in Dulbecco’s modified Eagle’s medium (DMEM) (GIBCO) supplemented with 1% penicillin/streptomycin double-antibody (GIBCO) and 10% fetal bovine serum (FBS, GIBCO) in a humidified 5% CO₂ incubator (Thermo) at 37 °C. After the medium was discarded, the cells were washed once with cold phosphate-buffered saline (PBS) and treated with pancreatin (GIBCO) at 37 °C for 2 min. The suspension was treated with complete medium to neutralize pancreatin, and the mixture was centrifuged (1000 rpm, 5 min). The supernatant was discarded and the cells were resuspended in FBS-supplemented DMEM and cultured in a humidified 5% CO₂ incubator (Thermo) at 37 °C.

Cell counting kit-8 (CCK-8) assay

The cells were counted, seeded into 96-well plates (ABI, 1 × 10⁴ cells/well), and cultured in a humidified 5% CO₂ incubator (Thermo) at 37 °C overnight. Following incubation, cells were treated with different concentrations of HPD (0, 2.5, 5, 10, 20, 30, 60, and 120 µg/mL) and

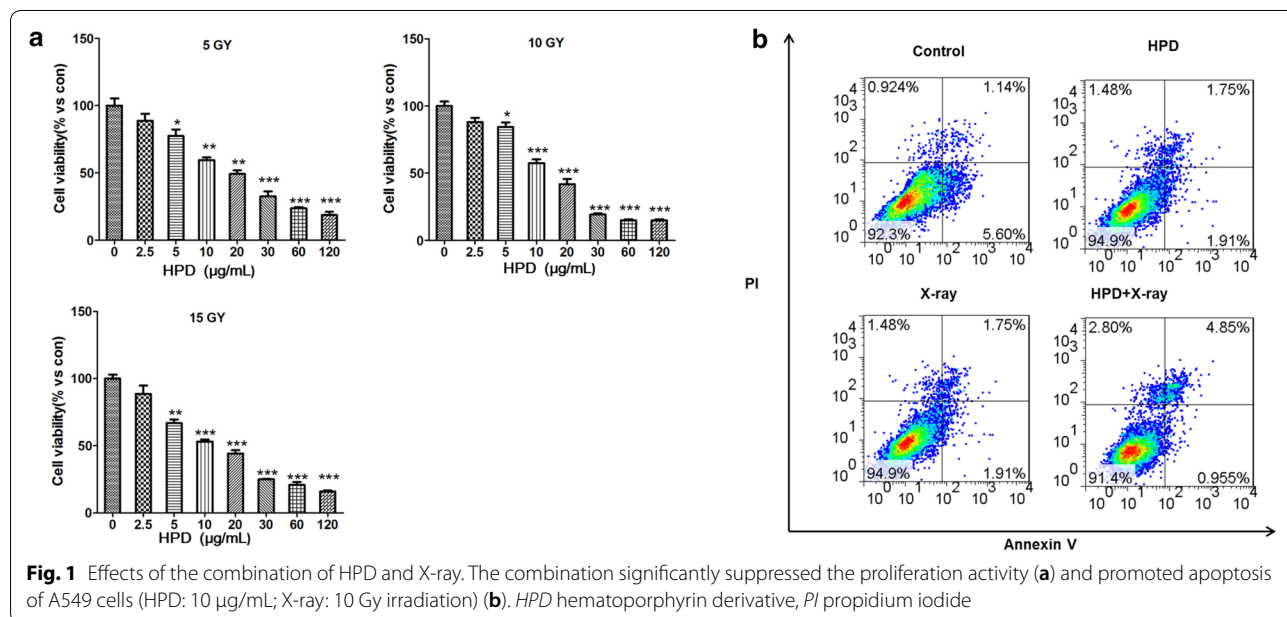


Table 1 The results of quality control for sequencing data

Sample	Raw reads	Raw base	Clean read	Clean base	Clean reads rate (%)	Clean reads mean length
C1_R1	23,719,333	3,557,899,950	22,042,930	2,960,605,850	92.93	134.3109038
C1_R2	23,719,333	3,557,899,950	19,989,260	2,662,625,066	84.27	133.2027832
C2_R1	34,224,122	5,133,618,300	32,282,452	4,221,477,560	94.33	130.766943
C2_R2	34,224,122	5,133,618,300	30,870,743	4,017,646,477	90.20	130.1441458
C3_R3	28,305,868	4,245,880,200	26,491,724	3,503,162,645	93.59	132.2361144
C3_R3	28,305,868	4,245,880,200	25,565,624	3,364,967,177	90.32	131.6207724
H1_R1	31,013,406	4,652,010,900	29,028,783	3,809,754,255	93.60	131.2405778
H1_R2	31,013,406	4,652,010,900	28,211,189	3,695,864,424	90.96	131.0070421
H2_R1	36,876,370	5,531,455,500	34,583,327	4,464,527,411	93.78	129.0947922
H2_R2	36,876,370	5,531,455,500	33,557,059	4,323,966,213	91.00	128.854147
H3_R1	31,602,257	4,740,338,550	29,790,898	3,839,171,450	94.27	128.8706185
H3_R2	31,602,257	4,740,338,550	28,994,009	3,728,257,975	91.75	128.5871842
X1_R1	38,506,430	5,775,964,500	36,323,284	4,706,649,914	94.33	129.5766626
X1_R2	38,506,430	5,775,964,500	35,392,852	4,573,185,587	91.91	129.2121242
X2_R1	26,676,689	4,001,503,350	24,977,453	3,294,932,070	93.63	131.9162554
X2_R2	26,676,689	4,001,503,350	23,234,815	3,048,373,656	87.10	131.1985336
X3_R1	26,125,305	3,918,795,750	24,664,499	3,184,364,078	94.41	129.1071867
X3_R2	26,125,305	3,918,795,750	23,447,530	3,013,771,864	89.75	128.5325944

Table 2 The results of mapping the sequencing data to human genome

Sample name	Left		Right		All pair	
	Mapped	Uniquely mapped	Mapped	Uniquely mapped	Mapped	Uniquely mapped
C1	20,710,400	18,614,230	17,931,401	16,062,833	2,123,508	1,629,067
C2	29,825,454	26,711,264	27,530,725	24,622,143	3,273,719	2,485,977
C3	24,351,734	22,204,068	23,021,298	21,001,313	2,555,418	1,941,532
X1	33,144,667	29,801,821	31,766,989	28,555,706	3,845,887	2,915,483
X2	23,108,910	20,910,087	20,617,622	18,640,706	2,428,431	1,848,198
X3	22,680,212	20,131,394	20,793,708	18,409,380	2,466,001	1,866,161
H1	26,599,811	23,805,716	25,426,744	22,751,212	2,999,459	2,248,238
H2	31,741,919	28,699,363	30,212,029	27,324,878	3,534,230	2,607,919
H3	27,165,798	24,935,225	25,977,523	23,876,280	2,940,041	2,153,962

different doses of X-ray (0, 5, 10, and 15 Gy; dose rate was 1 Gy/min) for 24 h. After treatment, the cells were incubated with CCK-8 solution (Tongren; 10 μ L/well) at 37 °C for 1 h. The absorbance value of each well was measured with BIV-TEK INSTRUMENTS INC (TECAN) at an optical density (OD) of 450 nm wavelength, and the cell proliferation activity was calculated.

Flow cytometry assay

To detect the apoptosis of A549 cells, flow cytometry assay was conducted according to the previously described method [15]. Cells were counted and cultured into six-well plates (ABI, 2×10^5 cells/well) in a humidified 5% CO₂ incubator (Thermo) at 37 °C

overnight. The cells were subsequently treated with different concentrations of HPD and different doses of X-ray. After the medium was discarded, the cells were digested with pancreatin (GIBCO), followed by treatment with fresh medium to deactivate pancreatin and centrifugation (1000 rpm, 6 min). The supernatant was discarded and the cells were washed once with PBS and resuspended in 1 \times binding buffer (BD Biosciences; 400 μ L 1 \times binding buffer for the control group and 100 μ L 1 \times binding buffer for other groups). A total of 100 μ L of the above solution was transferred into flow tubes and treated with 5 μ L of fluorescein isothiocyanate (FITC)-Annexin V (BD Biosciences) and 5 μ L of propidium iodide (PI, BD Biosciences, 50 μ g/mL) (the

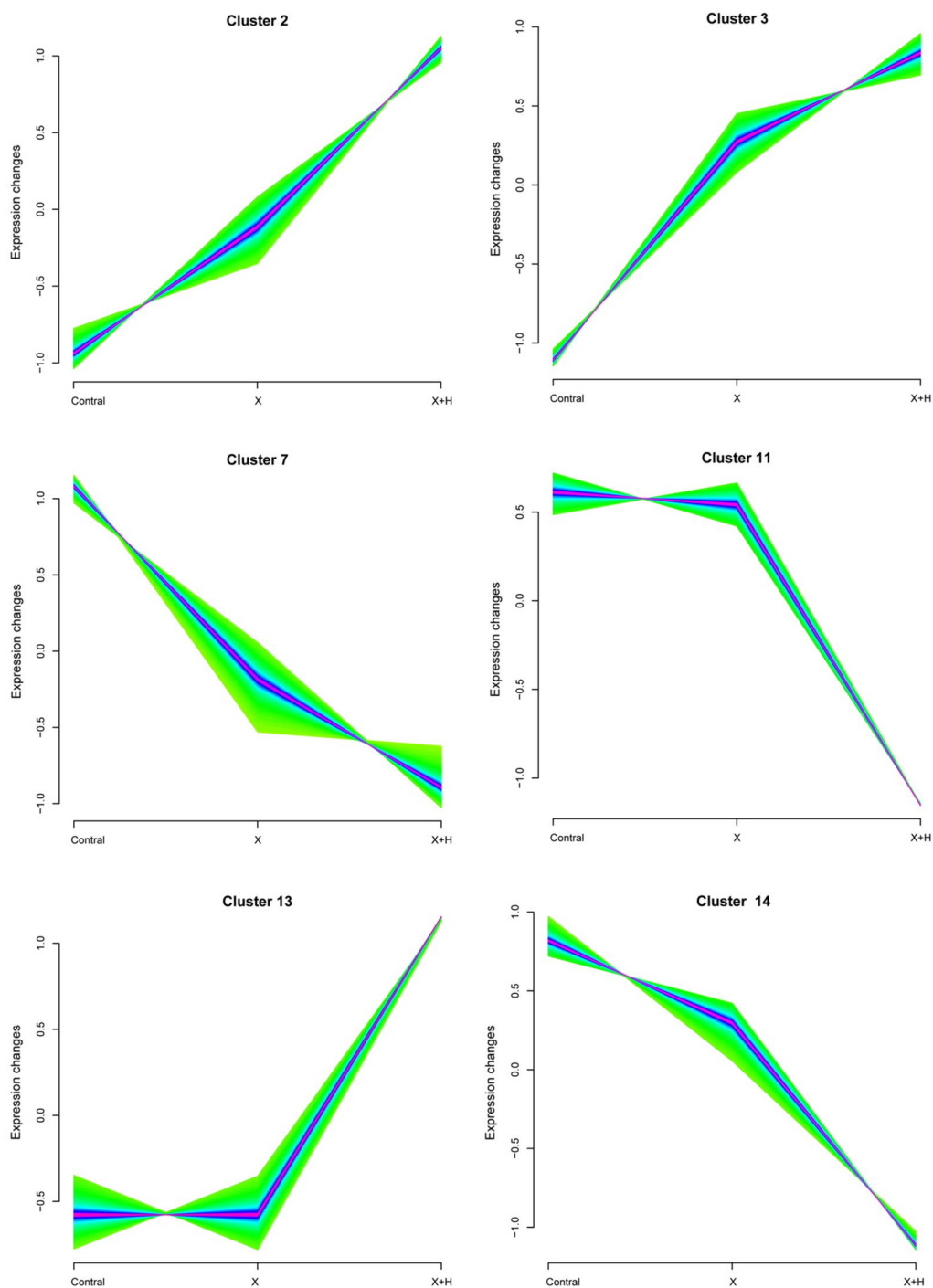
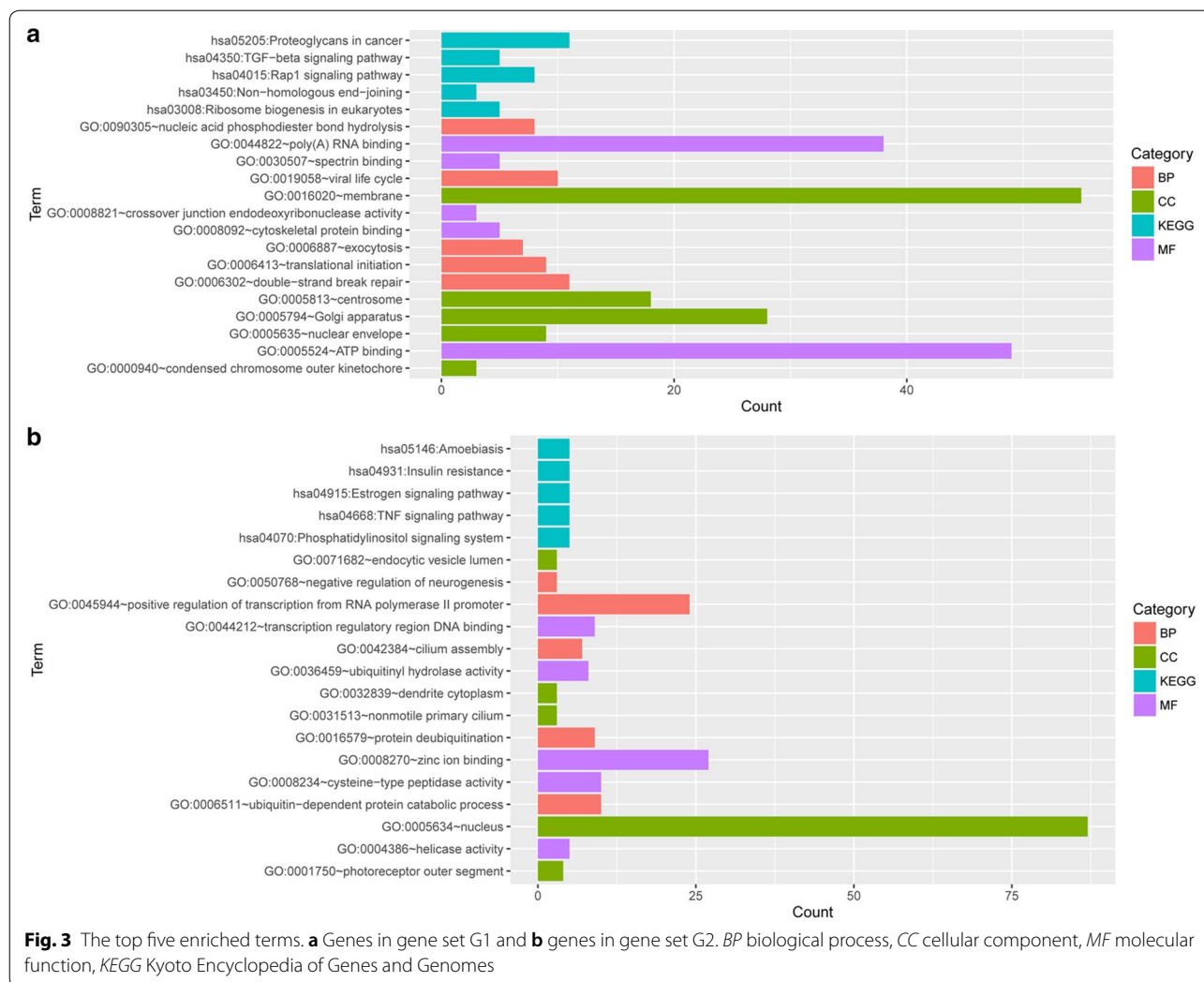


Fig. 2 The clusters 2, 3, 7, 11, 13, and 14 obtained from soft clustering analysis

control group was divided into unstained, Annexin V-stained, PI-stained, and Annexin V + PI-stained groups). After being incubated (in the absence of light) for 15 min at room temperature, the cells were treated with 400 μ L of $1 \times$ binding buffer (BD Biosciences) and analyzed with a flow cytometer (BD Biosciences).

RNA extraction and RNA-seq library construction

The cells were counted, seeded into 100 mm culture dishes (1×10^6 cells/well), and cultured in a humidified 5% CO_2 incubator (Thermo) at 37 $^\circ\text{C}$ overnight. After treatment with different concentrations of HPD or different doses of X-ray (the control group was left

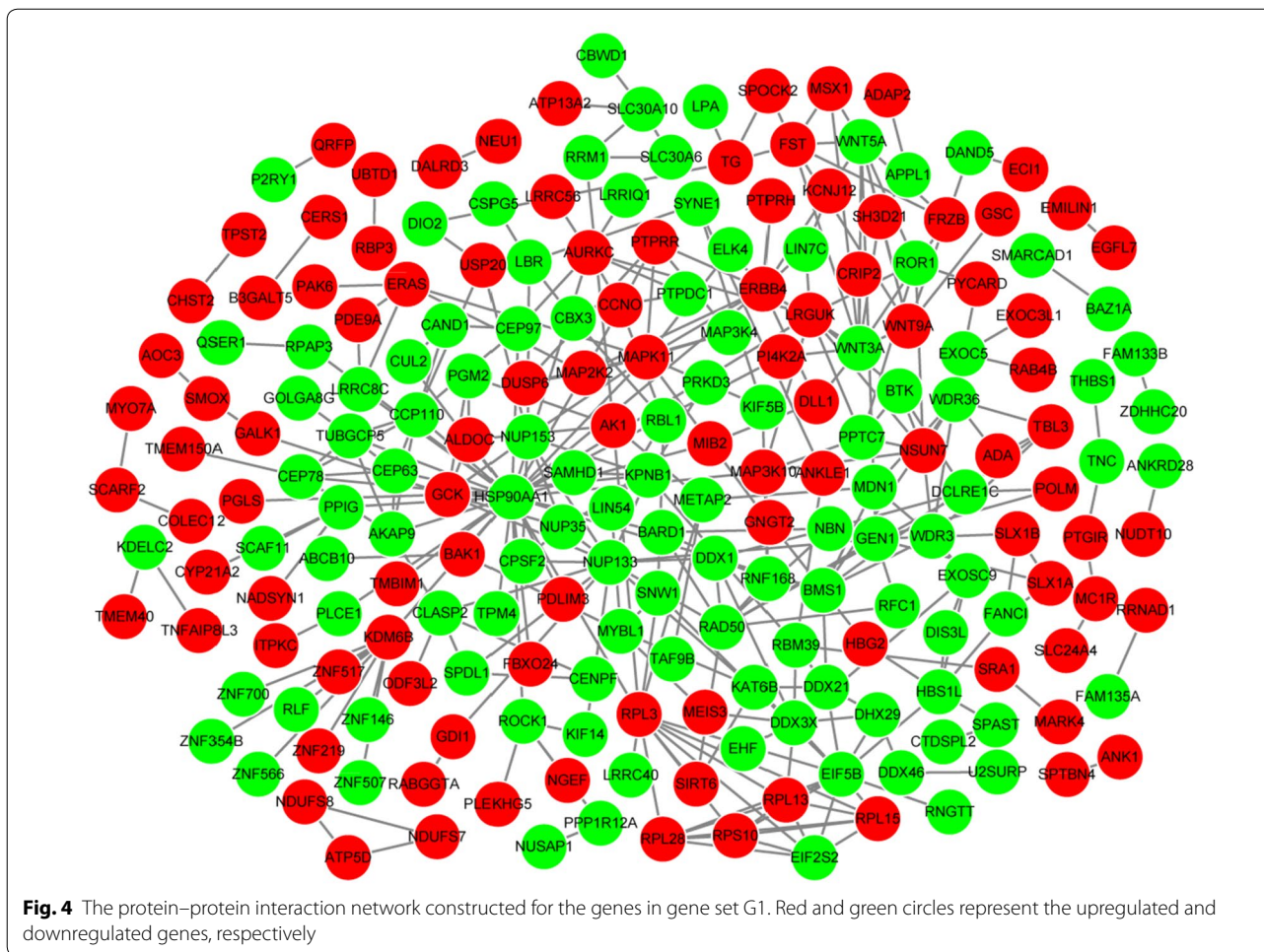


untreated; the X-ray group was treated with 10 Gy X-ray and cultured for 24 h; X-ray + HPD group was treated with 10 Gy X-ray + 10 µg/mL of HPD and cultured for 24 h; each group had three replicates), the cells were washed twice with cold PBS. Total RNA was extracted using Trizol reagent (TaKaRa) following the manufacturer’s instruction and quantified with a spectrophotometer (Nanodrop). RNA-seq library was constructed with NEBNext[®] Ultra[™] RNA Library Prep Kit for Illumina[®] (New England Biolabs) and sequencing was performed on Illumina HiSeq 4000 (PE150) (Illumina). The sequencing data were deposited into the Sequence Read Archive (SRA) database under the accession number of SRP091521.

Data preprocessing and DEG screening

The Prinseq-lite (<http://edwards.sdsu.edu/cgi-bin/prinseq/prinseq.cgi>) tool [16] and FASTX_ToolKit ([http://](http://hannonlab.cshl.edu/fastx_toolkit/)

hannonlab.cshl.edu/fastx_toolkit/) [17] were applied for the quality control of the raw data. Barcode and adaptor sequences in the reads were removed. The reads with N content larger than 5% were filtered out. Bases with continuous quality under 10 at 5’ or 3’ end were discarded. The reads with low quality (having over 20% bases with quality lower than 20) and those shorter than 30 nt were removed. The clean reads obtained from the three groups of samples were mapped to GRCH38 human genome using TopHat software (version 2.0.8) [18]. The fragments per kilobase million (FPKM) and read count matrix of the genes were acquired using StringTie tool [19], and gene annotation information was obtained from GENCODE database (version 24, <http://genome.imim.es/gencode/>) [20]. To identify DEGs, noise-robust soft clustering analysis was performed using the fuzzy c-means clustering algorithm in Mfuzz package (<http://www.bioconductor.org/packages/release/bioc/html/Mfuzz.html>) [21]. Specific clusters were selected based on gene expression



trends. Both minSTD and score parameters were set as 0.5.

Functional and pathway enrichment analysis

Gene ontology (GO, <http://www.geneontology.org>) database can use structured vocabularies for noting genes or gene products from three aspects (MF, molecular function; BP, biological process; and CC, cellular component) [22]. The Kyoto Encyclopedia of Genes and Genomes (KEGG, <http://www.genome.ad.jp/kegg>) database links genomic information with functional information through the investigation of gene functions [23]. “BioCloud” online tool (<http://www.biocloudservice.com>) is developed for settling computing problems of high-throughput biological data. Using “BioCloud” online tool, DEGs were subjected to GO functional and KEGG pathway enrichment analyses with the threshold of *p*-value < 0.05.

PPI network and module analyses

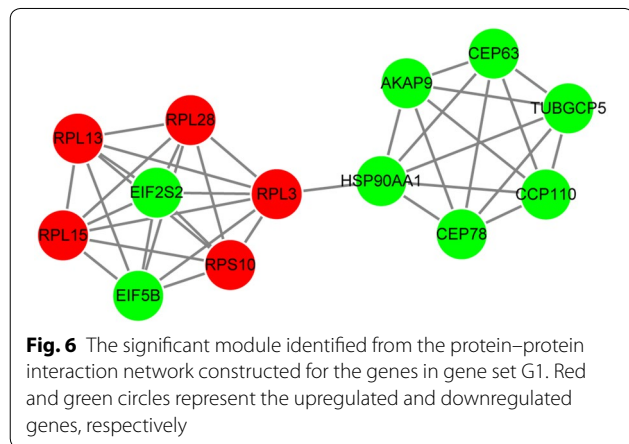
Search Tool for the Retrieval of Interacting Genes (STRING, <http://string-db.org/>) is a database that collects the PPIs involving more than 1100 organisms [24]. Based on STRING database [24], the PPIs among the proteins corresponding to DEGs were analyzed with a combined score > 0.4 as the cut-off criterion. PPI network was subsequently visualized using Cytoscape software (<http://www.cytoscape.org>) [25], and the hub nodes [26] in the PPI network were screened by calculating their connectivity degrees. Module analysis for PPI network was conducted using the Molecular Complex Detection (MCODE) plugin [27] of Cytoscape software. In addition, enrichment analysis was performed for the nodes of significant modules using “BioCloud” online tool.

Integrated network analysis

WEB-based gene set analysis toolkit (WebGestalt, <http://www.webgestalt.org>) [28] was used to predict the genes involved in the PPI network at *p* < 0.001 and the number

Table 3 The top 10 nodes in the protein–protein interaction networks constructed for the genes in gene set G1 and the genes in gene set G2

Gene set	Gene	Degree
Gene set G1	HSP90AA1	31
	NUP133	13
	EIF5B	12
	MAPK11	11
	ERBB4	10
	WNT3A	10
	RPL3	10
	DDX3X	9
	KDM6B	9
	GCK	9
Gene set G2	XRN1	14
	HSP90B1	13
	USP25	11
	ATM	8
	EPRS	7
	PIK3CB	7
	NCOA2	7
	CHD9	6
	PIAS1	6
	PIK3R1	5



Data preprocessing and DEG analysis

Data sequencing was carried out with quality control (Table 1), and the sequences were mapped to GRCH38 human genome (Table 2). The gene expression matrix was processed with Mfuzz package to reveal a total of 14 clusters (Fig. 2). According to the experimental design, only two types of clusters were selected for analysis. One type of clusters showed continuous upregulation (cluster 2 and 3) or downregulation (cluster 7 and 14) of gene expression along with the change in processing

conditions (untreated—treated with X-ray—treated with X-ray + HPD) (containing a total of 815 genes that were included in gene set G1). Another type of cluster included the significantly upregulated (cluster 13) or downregulated (cluster 11) genes under the processing condition of X-ray + HPD in comparison with the processing condition of untreated and X-ray treatment (containing a total of 464 genes that were included in gene set G2).

Functional and pathway enrichment analysis

The genes in gene set G1 and G2 were separately subjected to functional and pathway enrichment analyzes. The top five enriched terms in BP, CC, MF, and KEGG categories are shown in Fig. 3. The genes in gene set G1 were mainly enriched in double-strand break repair (BP), membrane (CC), ATP binding (MF), and proteoglycans in cancer (KEGG) (Fig. 3a). The genes in gene set G2 were mainly enriched in positive regulation of transcription from RNA polymerase II promoter (BP), nucleus (CC), zinc ion binding (MF), and estrogen signaling pathway (KEGG) (Fig. 3b).

PPI network and module analyses

The PPI network constructed for the genes in gene set G1 had 210 nodes and 333 interactions (Fig. 4). On the other hand, the PPI network constructed for the genes in gene set G2 had 135 nodes and 164 interactions (Fig. 5). The top 10 nodes with high degrees in PPI networks are listed in Table 3 and included heat shock protein 90 kDa alpha, class A member 1 (*HSP90AA1*, degree=31) and ribosomal protein L3 (*RPL3*, degree=10). Based on MCODE plugin, one significant module was identified from the PPI network constructed for the genes in gene set G1 that included 13 nodes and 37 interactions (such as *HSP90AA1-RPL3*) (Fig. 6). The terms enriched for the genes in the module are listed in Table 4, and mainly included translational initiation (BP, *p*-value=translational initiation), cytosol (CC, *p*-value=1.28E-09), poly(A) RNA binding (MF, *p*-value=1.70E-06), and ribosome (KEGG, *p*-value=4.57E-06). No significant module was identified from the PPI network constructed for the genes in gene set G2.

Integrated network analysis

The miRNAs of the genes implicated in the PPI networks constructed for the genes in gene set G1 (Table 5) and G2 (Table 6) were predicted. The TFs targeting the genes in gene set G1 (ATPase family, AAA domain containing 2 [*ATAD2*]) and G2 (protein inhibitor of activated STAT 1 [*PIAS1*]) were also analyzed (Table 7). An integrated network was constructed for the genes in gene set G1 that had 259 nodes (including 25 TFs and 31 miRNAs) and 687 pairs (Fig. 7). The

Table 4 The terms enriched for the genes in the significant module (only listed terms with p-value < 0.01)

Category	Term	Count	P-value	Gene symbol
BP	GO:0006413 ~ translational initiation	7	2.35E-10	RPL13, RPL15, EIF2S2, RPL3, EIF5B, RPS10, RPL28
BP	GO:0006412 ~ translation	7	2.20E-08	RPL13, RPL15, EIF2S2, RPL3, EIF5B, RPS10, RPL28
BP	GO:0000086 ~ G2/M transition of mitotic cell cycle	6	3.17E-08	HSP90AA1, TUBGCPS, CCP110, CEP78, AKAP9, CEP63
BP	GO:0006415 ~ translational termination	5	3.21E-07	RPL13, RPL15, RPL3, RPS10, RPL28
BP	GO:0016259 ~ selenocysteine metabolic process	5	3.70E-07	RPL13, RPL15, RPL3, RPS10, RPL28
BP	GO:0006414 ~ translational elongation	5	5.47E-07	RPL13, RPL15, RPL3, RPS10, RPL28
BP	GO:0006614 ~ SRP-dependent cotranslational protein targeting to membrane	5	8.12E-07	RPL13, RPL15, RPL3, RPS10, RPL28
BP	GO:0019083 ~ viral transcription	5	9.41E-07	RPL13, RPL15, RPL3, RPS10, RPL28
BP	GO:0001887 ~ selenium compound metabolic process	5	1.01E-06	RPL13, RPL15, RPL3, RPS10, RPL28
BP	GO:0000184 ~ nuclear-transcribed mRNA catabolic process, nonsense-mediated decay	5	1.20E-06	RPL13, RPL15, RPL3, RPS10, RPL28
BP	GO:0019058 ~ viral life cycle	5	3.22E-06	RPL13, RPL15, RPL3, RPS10, RPL28
BP	GO:0000278 ~ mitotic cell cycle	6	8.02E-06	HSP90AA1, TUBGCPS, CCP110, CEP78, AKAP9, CEP63
BP	GO:0044267 ~ cellular protein metabolic process	7	1.67E-05	RPL13, RPL15, EIF2S2, RPL3, EIF5B, RPS10, RPL28
BP	GO:0010467 ~ gene expression	7	2.65E-05	RPL13, RPL15, EIF2S2, RPL3, EIF5B, RPS10, RPL28
BP	GO:0006996 ~ organelle organization	5	4.52E-05	HSP90AA1, CCP110, CEP78, AKAP9, CEP63
BP	GO:0034641 ~ cellular nitrogen compound metabolic process	5	6.51E-05	RPL13, RPL15, RPL3, RPS10, RPL28
BP	GO:0016032 ~ viral process	5	4.78E-04	RPL13, RPL15, RPL3, RPS10, RPL28
BP	GO:0044281 ~ small molecule metabolic process	6	5.11E-03	HSP90AA1, RPL13, RPL15, RPL3, RPS10, RPL28
CC	GO:0005829 ~ cytosol	13	1.28E-09	HSP90AA1, TUBGCPS, CCP110, RPL13, CEP78, RPL15, EIF2S2, RPL3, EIF5B, RPS10, AKAP9, CEP63, RPL28
CC	GO:0022625 ~ cytosolic large ribosomal subunit	4	7.57E-06	RPL13, RPL15, RPL3, RPL28
CC	GO:0005813 ~ centrosome	5	1.28E-04	TUBGCPS, CCP110, CEP78, AKAP9, CEP63
CC	GO:0016020 ~ membrane	5	3.24E-02	HSP90AA1, RPL13, RPL15, RPS10, RPL28
CC	GO:0005840 ~ ribosome	2	3.80E-02	RPL15, RPS10
MF	GO:0044822 ~ poly(A) RNA binding	8	1.70E-06	HSP90AA1, RPL13, RPL15, EIF2S2, RPL3, EIF5B, RPS10, RPL28
MF	GO:0003735 ~ structural constituent of ribosome	5	7.88E-06	RPL13, RPL15, RPL3, RPS10, RPL28
MF	GO:0003723 ~ RNA binding	5	1.47E-04	RPL13, RPL15, EIF2S2, RPL3, RPL28
MF	GO:0005515 ~ protein binding	11	9.64E-03	HSP90AA1, CCP110, RPL13, RPL15, EIF2S2, RPL3, EIF5B, RPS10, AKAP9, CEP63, RPL28
KEGG	hsa03010 ~ ribosome	5	4.57E-06	RPL13, RPL15, RPL3, RPS10, RPL28

BP biological process, CC cellular component, MF molecular function, KEGG Kyoto Encyclopedia of Genes and Genomes

Table 5 The miRNAs targeted the genes implicated in the protein-protein interaction networks constructed for the genes in gene set G1

microRNA	Count	Statistics
hsa_TATTATA, MIR-374	9	p-value = 1.15e-05
hsa_CAGTATT, MIR-200B, MIR-200C, MIR-429	11	p-value = 1.92e-05
hsa_GTGCAAT, MIR-25, MIR-32, MIR-92, MIR-363, MIR-367	8	p-value = 1.00e-04
hsa_CTTTGTA, MIR-524	9	p-value = 0.0003
hsa_GGCACTT, MIR-519E	5	p-value = 0.0003
hsa_CTACTGT, MIR-199A	6	p-value = 0.0003
hsa_GCAAGGA, MIR-502	4	p-value = 0.0004
hsa_TGTTTAC, MIR-30A-5P, MIR-30C, MIR-30D, MIR-30B, MIR-30E-5P	10	p-value = 0.0005
hsa_TGAATGT, MIR-181A, MIR-181B, MIR-181C, MIR-181D	9	p-value = 0.0006
hsa_TGCTGCT, MIR-15A, MIR-16, MIR-15B, MIR-195, MIR-424, MIR-497	10	p-value = 0.0007
hsa_TACTTGA, MIR-26A, MIR-26B	7	p-value = 0.0007
hsa_ATGTCAC, MIR-489	4	p-value = 0.0008

Table 6 The miRNAs targeted the genes implicated in the protein–protein interaction networks constructed for the genes in gene set G2

microRNA	Count	Statistics
hsa_CAGTATT, MIR-200B, MIR-200C, MIR-429	13	<i>p</i> -value = 1.27e-09
hsa_CATTCA, MIR-203	10	<i>p</i> -value = 1.29e-08
hsa_TACTTGA, MIR-26A, MIR-26B	8	<i>p</i> -value = 2.86e-06
hsa_ATGTACA, MIR-493	8	<i>p</i> -value = 4.11e-06
hsa_AAGCACT, MIR-520F	7	<i>p</i> -value = 6.53e-06
hsa_ATTCTTT, MIR-186	7	<i>p</i> -value = 1.56e-05
hsa_GCTGAGT, MIR-512-5P	4	<i>p</i> -value = 1.69e-05
hsa_GTACAGG, MIR-486	4	<i>p</i> -value = 2.43e-05
hsa_AAAGGGA, MIR-204, MIR-211	6	<i>p</i> -value = 4.87e-05
hsa_TGCTGCT, MIR-15A, MIR-16, MIR-15B, MIR-195, MIR-424, MIR-497	9	<i>p</i> -value = 6.55e-05
hsa_TGGTGCT, MIR-29A, MIR-29B, MIR-29C	8	<i>p</i> -value = 1.00e-04
hsa_ATGTTTC, MIR-494	5	<i>p</i> -value = 1.00e-04
hsa_GTGCAAT, MIR-25, MIR-32, MIR-92, MIR-363, MIR-367	6	<i>p</i> -value = 0.0003
hsa_CTGTAC, MIR-194	4	<i>p</i> -value = 0.0003
hsa_CTATGCA, MIR-153	5	<i>p</i> -value = 0.0004
hsa_ACTGTAG, MIR-139	4	<i>p</i> -value = 0.0005
hsa_CTGAGCC, MIR-24	5	<i>p</i> -value = 0.0006

Table 7 The transcription factors (TFs) targeting the genes in gene set G1 and gene set G2

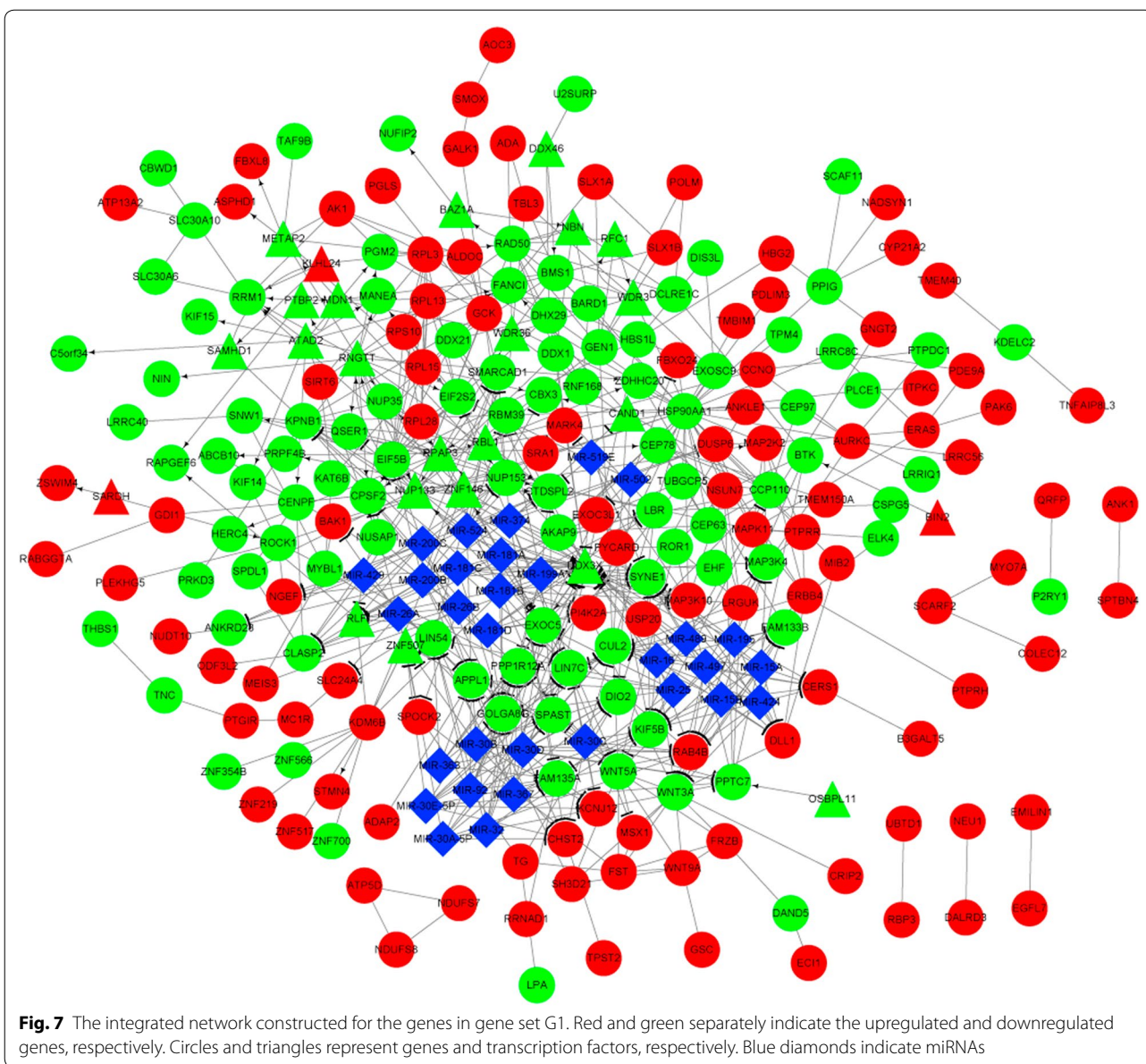
G1 gene list		G2 gene list	
TF	Count	TF	Count
<i>RNGTT</i>	14	<i>TRIM23</i>	7
<i>RPAP3</i>	13	<i>NCOA2</i>	6
<i>ATAD2</i>	10	<i>PHC3</i>	4
<i>ZNF146</i>	6	<i>SYNJ1</i>	4
<i>NUP133</i>	5	<i>CHD9</i>	3
<i>METAP2</i>	4	<i>PIAS1</i>	3
<i>RBL1</i>	4	<i>BAZ2B</i>	2
<i>DDX3X</i>	3	<i>EPRS</i>	2
<i>KLHL24</i>	3	<i>MRPS12</i>	2
<i>PTBP2</i>	3	<i>PSME4</i>	2
<i>BAZ1A</i>	2	<i>PWWP2B</i>	2
<i>CAND1</i>	2	<i>MIER1</i>	1
<i>MDN1</i>	2	<i>TCF12</i>	1
<i>SARDH</i>	2	<i>TTC3</i>	1
<i>WDR36</i>	2	<i>ZBTB33</i>	1
<i>BIN2</i>	1	<i>ZNF292</i>	1
<i>DDX46</i>	1	<i>ZNF593</i>	1
<i>NBN</i>	1		
<i>OSBPL11</i>	1		
<i>RFC1</i>	1		
<i>RLF</i>	1		
<i>SAMHD1</i>	1		
<i>WDR3</i>	1		
<i>ZNF507</i>	1		

integrated network for the genes in gene set G2 was also visualized; it carried 174 nodes (including 18 TFs and 32 miRNAs) and 445 pairs (Fig. 8). In particular, ubiquitin-specific peptidase 25 (*USP25*) was targeted by *miR-200b*, *miR-200c*, and *miR-429* in the integrated network for the genes in gene set G2. The top 30 nodes with high degrees in the integrated networks are listed in Table 8.

Discussion

In this study, the CCK-8 assay result revealed the significant suppression in the proliferation activity of A549 cells in response to the treatment with the combination of HPD and X-ray. The combination of 10 µg/mL of HPD and 10 Gy X-ray was selected as the lowest concentration/dose that achieved a significant increase in the apoptosis of A549 cells, which might be a limitation in terms of analysis of the data. In Europe, hematoporphyrin is the most commonly used photosensitizer for the treatment of advanced lung cancer [30, 31]. Previous studies have demonstrated that HPD-PDT may inhibit proliferation and induce apoptosis of A549 cells, thereby inducing effective killing of adenocarcinoma cells [32, 33]. After the optimization of the combination treatment of HPD and X-ray, a series of bioinformatic analyses were performed with the RNA-seq data.

Through noise-robust soft clustering analysis, 815 genes that showed continuous upregulated or downregulated expression along with the change in processing conditions (untreated—treated with X-ray—treated



with X-ray+HPD) were included in the gene set G1. A total of 464 genes that were significantly upregulated or downregulated under the processing condition of X-ray+HPD were included in the gene set G2. The significant module identified from the PPI network constructed for the genes in gene set G1 revealed the interaction between *RPL3* and *HSP90AA1*. *RPL3* functions in the response of cells to oxaliplatin- and 5-fluorouracil-induced nucleolar stress and may be used to improve the therapeutic effects of these drugs against cancers [34]. The chemotherapy curative effect of actinomycin D is determined by *RPL3* status in cancers shorting of *p53*; thus, high level of *RPL3* may be useful for the treatment of lung and colon cancers [35].

The frequencies of mutant genotypes of *HSP90AA1*, *HSP90AB1*, and *HSP90B1* are reported to be significantly higher in the patients with non-small cell lung cancer (NSCLC) in the Turkish population [36]. Downregulation of *HSP90* expression correlated with increased overall survival of patients with NSCLC, and *HSP90* inhibitor exerts an antiproliferative effect on NSCLC cell lines [37, 38]. These observations suggest that *RPL3* interacting with *HSP90AA1* may be associated with the sensibilization effect of HPD in lung adenocarcinoma.

ATAD2 and *PIAS1* were separately predicted as the TFs targeting the genes from the gene sets G1 and G2. Caron et al. demonstrated that *ATAD2* overexpression

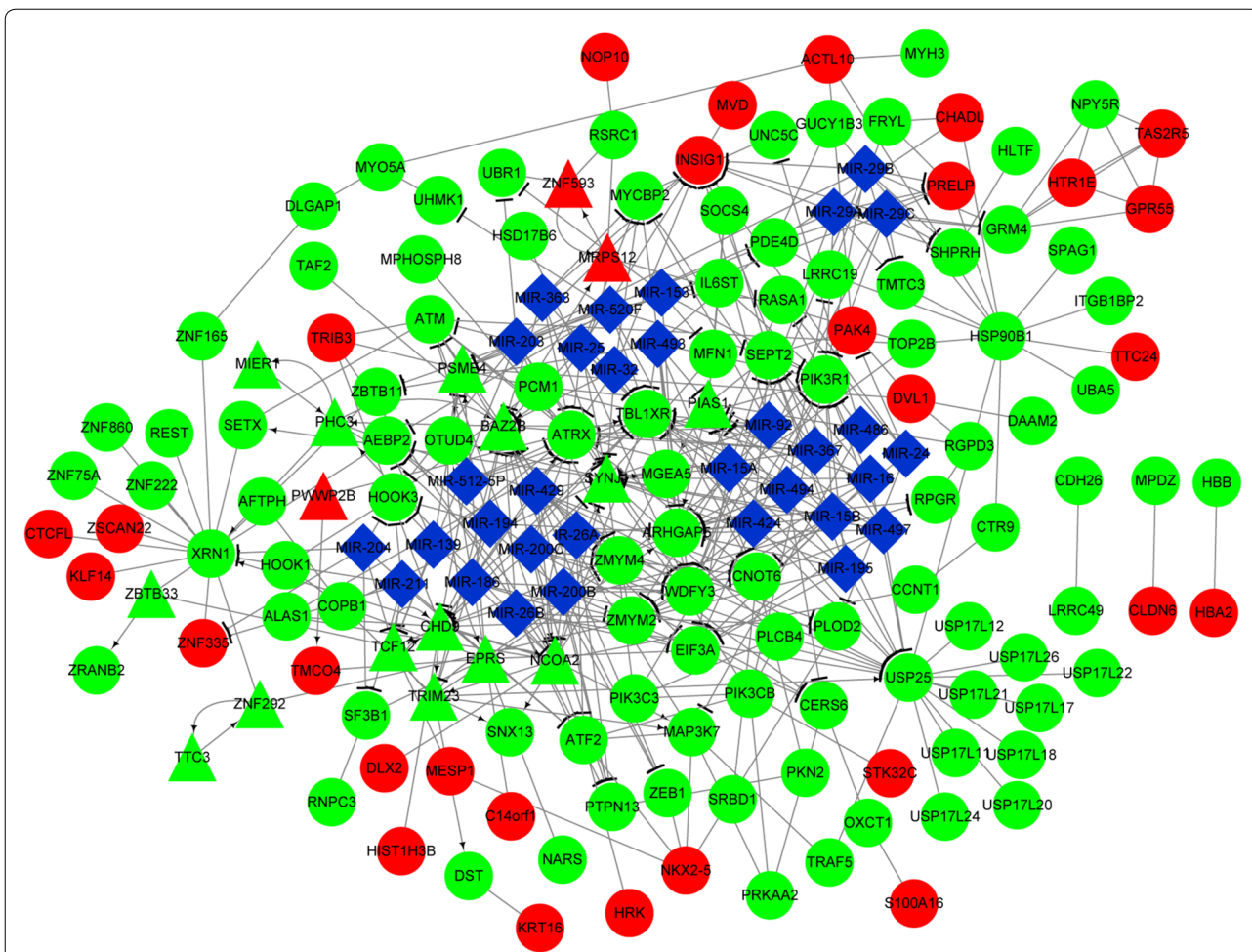


Fig. 8 The integrated network constructed for the genes in gene set G2. Red and green separately indicate the upregulated and downregulated genes, respectively. Circles and triangles indicate genes and transcription factors, respectively. Blue diamonds indicate miRNAs

may promote the malignant transformation of lung and breast cancers by affecting the basic properties of chromatin [39]. Wang et al. found that ATAD2/AAA⁺ nuclear coregulatory cancer associated (*ANCCA*) may serve as a promising biomarker for the treatment and prognosis of squamous cell lung carcinoma [40]. *PIAS1* contributes to cytoplasm-nuclear distribution of focal adhesion kinase by interacting with it, and focal adhesion kinase activity in the nucleus facilitates survival and progression of NSCLC via promotion of DNA repair regulation and cell-extracellular matrix interaction [41, 42]. *PIAS1* mediates oncogenic signaling by promoting promyelocytic leukemia (PML) degradation, and *PIAS1* and PML expression is negatively correlated in NSCLC cell lines [43]. Therefore, *ATAD2* and *PIAS1* may be involved in the action mechanism of HPD in lung adenocarcinoma.

In the integrated network for the genes in the gene set G2, *USP25* was targeted by *miR-200b*, *miR-200c*, and *miR-429*. *miR-200c* may serve as a tumor

suppressor in NSCLC through the inhibition of *USP25* expression and may be applied for therapeutic purposes [44]. The overexpression of *miR-200c* and *miR-141* is associated with the short overall survival of patients with lung adenocarcinoma via angiogenesis and mesenchymal-epithelial transition [45]. The low expression of *miR-200b* is reported to induce E2F transcription factor 3 overexpression and increase the chemoresistance of patients with lung adenocarcinoma to docetaxel [46]. Zhu et al. suggested that the serum levels of *miR-29c* and *miR-429* may be used as non-invasive biomarkers for patients with early stage NSCLC [47]. Lang et al. found that *miR-429* contributes to cell proliferation and metastasis and regulates several tumor suppressor genes in patients with NSCLC, serving as a possible therapeutic target [48]. These observations suggest that *USP25* targeted by *miR-200b*, *miR-200c*, and *miR-429* may also function in the action process of HPD in lung adenocarcinoma.

Table 8 The top 30 nodes with higher degrees in the integrated networks for gene set G1 and gene set G2

G1 gene list		G2 gene list	
Node	Degree	Node	Degree
<i>DDX3X</i>	34	<i>SYNJ1</i>	25
<i>HSP90AA1</i>	31	<i>USP25</i>	23
<i>NUP133</i>	21	<i>TBL1XR1</i>	21
<i>RPAP3</i>	19	<i>NCOA2</i>	20
<i>RNGTT</i>	17	<i>PIK3R1</i>	18
<i>WNT3A</i>	16	<i>XRN1</i>	18
<i>SYNE1</i>	15	<i>CHD9</i>	17
<i>EIF5B</i>	15	<i>BAZ2B</i>	17
<i>GOLGA8G</i>	14	<i>PIAS1</i>	16
<i>KIF5B</i>	14	<i>ATRX</i>	14
<i>EXOC5</i>	14	<i>ARHGAP5</i>	14
<i>WNT5A</i>	13	<i>MIR-200B</i>	13
<i>PPP1R12A</i>	13	<i>MIR-200C</i>	13
<i>CUL2</i>	13	<i>MIR-429</i>	13
<i>LIN7C</i>	13	<i>HSP90B1</i>	13
<i>NUP153</i>	12	<i>WDFY3</i>	12
<i>RAB4B</i>	12	<i>TRIM23</i>	12
<i>MIR-200B</i>	11	<i>INSIG1</i>	11
<i>CTDSPL2</i>	11	<i>ATM</i>	11
<i>RLF</i>	11	<i>SEPT2</i>	11
<i>APPL1</i>	11	<i>MIR-203</i>	10
<i>MIR-200C</i>	11	<i>PSME4</i>	10
<i>MIR-429</i>	11	<i>EIF3A</i>	10
<i>PPTC7</i>	11	<i>ZMYM2</i>	10
<i>MIR-30B</i>	11	<i>EPRS</i>	10
<i>KPNB1</i>	11	<i>CNOT6</i>	9
<i>MAPK11</i>	11	<i>ATF2</i>	9
<i>EIF2S2</i>	10	<i>MIR-15A</i>	9
<i>CLASP2</i>	10	<i>MIR-16</i>	9
<i>DLL1</i>	10	<i>MIR-15B</i>	9

Conclusion

A total of 815 DEGs in gene set G1 were identified along with a change in processing conditions (untreated—treated with X-ray—treated with X-ray + HPD). In addition, 464 DEGs in gene set G2 were screened under the processing condition of X-ray + HPD. *RPL3*, *HSP90AA1*, *ATAD2*, as well as *PIAS1* and *USP25*, which is targeted by *miR-200b*, *miR-200c*, and *miR-429* may show correlations with the sensibilization effect of HPD in lung adenocarcinoma. Further validation with experimental research is warranted to confirm the roles of these genes in the sensibilization effect of HPD in lung adenocarcinoma.

Highlights

1. In the significant module for gene set G1, *RPL3* could interact with *HSP90AA1*.
2. *ATAD2* and *PIAS1* were the transcription factors separately targeting the gene set G1 and G2.
3. In the integrated network, *miR-200b*, *miR-200c*, and *miR-429* co-regulated *USP25*.

Abbreviations

HPD: hematoporphyrin derivative; DEGs: differentially expressed genes; PPI: protein–protein interaction; ITFP: integrated transcription factor platform; TF: transcription factor; PDT: photodynamic therapy; X-PDT: X-ray-induced photodynamic therapy; DMEM: Dulbecco's modified Eagle's medium; PBS: phosphate-buffered saline; CCK-8: cell counting kit-8; FITC: fluorescein isothiocyanate; FPKM: fragments per kilobase million.

Authors' contributions

HY carried out the conception and design of the research, participated in the acquisition of data, and drafted the manuscript. YY carried out the analysis and interpretation of data, participated in the study design, and performed statistical analyses. Both authors read and approved the final manuscript.

Author details

¹ Department of Radiation Oncology, Harbin Medical University Cancer Hospital, Harbin 150081, Heilongjiang, China. ² Department of Medical Oncology, Harbin Medical University Cancer Hospital, No. 150 Haping Road, Nangang District, Harbin 150081, Heilongjiang, China.

Acknowledgements

Not applicable.

Competing interests

The authors declare that they have no competing interests.

Availability of data and materials

The sequencing data were deposited into the Sequence Read Archive (SRA) database under the Accession Number of SRP091521.

Consent for publication

Not applicable.

Ethics approval and consent to participate

This study was approved by Ethics Committee of Harbin Medical University Cancer Hospital.

Funding

None.

Publisher's Note

Springer Nature remains neutral with regard to jurisdictional claims in published maps and institutional affiliations.

Received: 7 September 2018 Accepted: 16 January 2019
Published online: 04 February 2019

References

1. Lortet-Tieulent J, Soerjomataram I, Ferlay J, Rutherford M, Weiderpass E, Bray F. International trends in lung cancer incidence by histological subtype: adenocarcinoma stabilizing in men but still increasing in women. *Lung Cancer*. 2014;84(1):13–22.

2. Ahrendt SA, Decker PA, Alawi EA, Zhu YR, Sanchez-Cespedes M, Yang SC, Haasler GB, Kajdacsy-Balla A, Demeure MJ, Sidransky D. Cigarette smoking is strongly associated with mutation of the K-ras gene in patients with primary adenocarcinoma of the lung. *Cancer*. 2001;92(6):1525–30.
3. Rivera GA, Wakelee H. Lung cancer in never smokers. *Oxygen Transport Tissue XXXIII*. 2016;893(10):43–57.
4. Mcguire S. World Cancer Report 2014. Geneva, Switzerland: World Health Organization, International Agency for Research on Cancer, WHO Press, 2015. *Adv Nutr*. 2016; 7(2):418.
5. Marugame T, Sobue T, Nakayama T, Suzuki T, Kuniyoshi H, Sunagawa K, Genka K, Nishizawa N, Natsukawa S, Kuwahara O. Filter cigarette smoking and lung cancer risk; a hospital-based case-control study in Japan. *Br J Cancer*. 2004;90(3):646–51.
6. Verdu M, Trias I, Roman R, Rodon N, Pubill C, Calvo M, Garcia-Pelaez B, Diaz O, Puig X. EGFR mutations in lung cancer: a morphological, immunohistochemical and molecular study of lung adenocarcinoma. *Revista Española De Patología*. 2016;49(4):226–33.
7. Fh F, Gs W, Lo M. Cancer detection and therapy; affinity of neoplastic, embryonic, and traumatized tissues for porphyrins and metalloporphyrins. *Proc Soc Exp Biol Med Soc Exp Biol Med*. 1948;68(3):640.
8. Li W, Yang J, Zheng S, Wen J, Zhai M, Liu Y. The study of comparing the efficiency of ZnPC-PDT and HPD-PDT in killing mice lewis lung cancer cells. *Ibmbe Proc*. 2013;39:1644–7.
9. Yang SG, Chang JE, Shin B, Park S, Na K, Shim CK. 99mTc-hematoporphyrin linked albumin nanoparticles for lung cancer targeted photodynamic therapy and imaging. *J Mater Chem*. 2010;20(41):9042–6.
10. Wang Y, Lin Y, Zhang HG, Zhu J. A photodynamic therapy combined with topical 5-aminolevulinic acid and systemic hematoporphyrin derivative is more efficient but less phototoxic for cancer. *J Cancer Res Clin Oncol*. 2016;142(4):1–9.
11. Novichenko NL, Mamchur AA, Lisniak IO, Gamaliya MF. Study of photodynamic efficiency of the hematoporphyrin conjugated with antibody to VEGF in mouse Lewis carcinoma. *Exp Oncol*. 2008;30(4):315–8.
12. Usuda J, Okunaka T, Furukawa K, Tsuchida T, Kuroiwa Y, Ohe Y, Saijo N, Nishio K, Konaka C, Kato H. Increased cytotoxic effects of photodynamic therapy in IL-6 gene transfected cells via enhanced apoptosis. *Int J Cancer*. 2001;93(4):475–80.
13. Wang GD, Nguyen HT, Chen H, Cox PB, Wang L, Nagata K, Hao Z, Wang A, Li Z, Xie J. X-ray induced photodynamic therapy: a combination of radiotherapy and photodynamic therapy. *Theranostics*. 2016;6(13):2295–305.
14. Austerlitz C, Souza VLBD, Campos DMT, Kurachi C, Bagnato V, Sibata C. Enhanced response of the Fricke solution doped with hematoporphyrin under X-rays irradiation. *Braz Archiv Biol Technol*. 2008;51(2):271–9.
15. Lutsenko GV. Flow-cytometry assay for apoptosis using fluorophor 10-N-nonyl acridine orange. *Biochem Suppl*. 2010;4(4):349–57.
16. Schmieder R, Edwards R. Quality control and preprocessing of metagenomic datasets. *Bioinformatics*. 2011;27(27):863–4.
17. Krueger F, Kreck B, Franke A, Andrews SR. DNA methylome analysis using short bisulfite sequencing data. *Nat Methods*. 2012;9(2):145–51.
18. Kim D, Pertea G, Trapnell C, Pimentel H, Kelley R, Salzberg SL. TopHat2: accurate alignment of transcriptomes in the presence of insertions, deletions and gene fusions. *Genome Biol*. 2013;14(4):R36.
19. Pertea M, Pertea GM, Antonescu CM, Chang TC, Mendell JT, Salzberg SL. StringTie enables improved reconstruction of a transcriptome from RNA-seq reads. *Nat Biotechnol*. 2015;33(3):290–5.
20. Harrow J, Frankish A, Gonzalez JM, Tapanari E, Diekhans M, Kokocinski F, Aken BL, Barrell D, Zadissa A, Searle S. GENCODE: the reference human genome annotation for The ENCODE Project. *Genome Res*. 2012;22(9):1760–74.
21. Futschik ME, Carlisle B. Noise-robust soft clustering of gene expression time-course data. *J Bioinform Comput Biol*. 2005;3(4):965–88.
22. Consortium TGO. Gene Ontology Consortium: going forward. *Nucl Acids Res*. 2015;43(Database issue):1049–56.
23. Kanehisa M, Sato Y, Kawashima M, Furumichi M, Tanabe M. KEGG as a reference resource for gene and protein annotation. *Nucleic Acids Res*. 2015;44(D1):D457–62.
24. Franceschini A, Szklarczyk D, Frankild S, Kuhn M, Simonovic M, Roth A, Lin J, Minguez P, Bork P, von Mering C. STRING v9. 1: protein-protein interaction networks, with increased coverage and integration. *Nucleic Acids Res*. 2013;41(D1):D808–15.
25. Saito R, Smoot ME, Ono K, Ruscheinski J, Wang P-L, Lotia S, Pico AR, Bader GD, Ideker T. A travel guide to Cytoscape plugins. *Nat Methods*. 2012;9(11):1069–76.
26. Liu X, Wang Y, Zhao D, Zhang W, Shi L. Patching by automatically tending to hub nodes based on social trust. *Comput Stand Interf*. 2016;44:94–101.
27. Bader GD, Hogue CW. An automated method for finding molecular complexes in large protein interaction networks. *BMC Bioinform*. 2003;4:2.
28. Wang J, Duncan D, Shi Z, Zhang B. WEB-based Gene Set Analysis Toolkit (WebGestalt): update 2013. *Nucleic Acids Res*. 2013;41(W1):77–83.
29. Zheng G. ITFP: an integrated platform of mammalian transcription factors. *Bioinformatics*. 2008;24(20):2416–7.
30. Almeida RD, Manadas BJ, Carvalho AP, Duarte CB. Intracellular signaling mechanisms in photodynamic therapy. *Biochem Biophys Acta*. 2004;1704(2):59.
31. Dougherty TJ. An update on photodynamic therapy applications. *J Clin Laser Med Surg*. 2002;20(1):3–7.
32. Yang ZZ, Li MY, Xiang DB, Dai N, Zeng LL, Li ZP, Wang G, Wang D. Knock down of the dual functional protein apurinic/aprimidinic endonuclease 1 enhances the killing effect of hematoporphyrin derivative-mediated photodynamic therapy on non-small cell lung cancer cells in vitro and in a xenograft model. *Cancer Sci*. 2010;101(1):180.
33. Xia L, Guan W, Wang D, Zhang YS, Zeng LL, Li ZP, Wang G, Yang ZZ. Killing effect of Ad5/F35-APE1 siRNA recombinant adenovirus in combination with hematoporphyrin derivative-mediated photodynamic therapy on human non-small cell lung cancer. *Biomed Res Int*. 2013;2013(4):957913.
34. Esposito D, Crescenzi E, Sagar V, Loreni F, Russo A, Russo G. Human rPL3 plays a crucial role in cell response to nucleolar stress induced by 5-FU and L-OHP. *Oncotarget*. 2014;5(22):11737–51.
35. Russo A, Pagliara V, Albano F, Esposito D, Sagar V, Loreni F, Irace C, Santamaria R, Russo G. Regulatory role of rPL3 in cell response to nucleolar stress induced by Act D in tumor cells lacking functional p53. *Cell Cycle*. 2015;15(1):41–51.
36. Coskuncpinar E, Akkaya N, Yildiz P, Oltulu YM, Aynaci E, Isbir T, Yaylim I. The significance of HSP90AA1, HSP90AB1 and HSP90B1 gene polymorphisms in a Turkish population with non-small cell lung cancer. *Anticancer Res*. 2014;34(2):753–7.
37. Ruiz MIG, Floor K, Roepman P, Rodriguez JA, Meijer GA, Mooi WJ, Jansen E, Niklinski J, Muley T, Van Zandwijk N. Integration of gene dosage and gene expression in non-small cell lung cancer, identification of HSP90 as potential target. *PLoS ONE*. 2008;3(3):e1722.
38. Sequist LV, Gettinger S, Senzer NN, Martins RG, Jänne PA, Lilenbaum R, Gray JE, Iafrate AJ, Katayama R, Hafeez N. Activity of IPI-504, a novel heat-shock protein 90 inhibitor, in patients with molecularly defined non-small-cell lung cancer. *J Clin Oncol*. 2010;28(33):4953–60.
39. Caron C, Lestrat C, Marsal S, Escoffier E, Curtet S, Virolle V, Barbry P, Debernardi A, Brambilla C, Brambilla E. Functional characterization of ATAD2 as a new cancer/testis factor and a predictor of poor prognosis in breast and lung cancers. *Oncogene*. 2010;29(37):5171–81.
40. Wang D, Pan Y, Hao T, Chen Y, Qiu S, Chen L, Zhao J. Clinical and prognostic significance of ANCCA in squamous cell lung carcinoma patients. *Arch Med Res*. 2016;47(2):89–95.
41. Constanzo JD, Tang KJ, Rindhe S, Melegari M, Liu H, Tang X, Rodriguez-Canales J, Wistuba I, Scagliioni PP. PIAS1-FAK interaction promotes the survival and progression of non-small cell lung cancer. *Neoplasia*. 2016;18(5):282–93.
42. Constanzo JD, Rabellino A, Konstantinidou S, Scagliioni K. The SUMO ligase PIAS1 promotes the progression and survival of solid tumors of different histopathological origins. *Int J Media Manag*. 2003;14(1):316.
43. Rabellino A, Carter B, Konstantinidou G, Wu SY, Rimessi A, Byers LA, Heymach JV, Girard L, Chiang CM, Teruya-Feldstein J. The SUMO E3-ligase PIAS1 regulates the tumor suppressor PML and its oncogenic counterpart PML-RARA. *Cancer Res*. 2012;72(9):2275–84.
44. Jing L, Qiang T, Yan M, Lei L, Lin H, Zhao F, Bao G, Kong H, Chao G, Zhang F. miRNA-200c inhibits invasion and metastasis of human non-small cell lung cancer by directly targeting ubiquitin specific peptidase 25. *Mol Cancer*. 2014;13(1):207–12.
45. Tejero R, Navarro A, Campayo M, Viñolas N, Marrades RM, Cordeiro A, Ruizmartinez M, Santasusagna S, Molins L, Ramirez J. miR-141 and miR-200c as markers of overall survival in early stage non-small cell lung cancer adenocarcinoma. *PLoS ONE*. 2014;9(7):e101899.

46. Feng B, Wang R, Song HZ, Chen LB. MicroRNA-200b reverses chemoresistance of docetaxel-resistant human lung adenocarcinoma cells by targeting E2F3. *Cancer*. 2012;118(13):3365–76.
47. Zhu W, He J, Chen D, Zhang B, Xu L, Ma H, Liu X, Zhang Y, Le H. Expression of miR-29c, miR-93, and miR-429 as potential biomarkers for detection of early stage non-small lung cancer. *PLoS ONE*. 2014;9(2):e87780.
48. Lang Y, Xu S, Ma J, Wu J, Jin S, Cao S, Yu Y. MicroRNA-429 induces tumorigenesis of human non-small cell lung cancer cells and targets multiple tumor suppressor genes. *Biochem Biophys Res Commun*. 2014;450(1):154–9.

Ready to submit your research? Choose BMC and benefit from:

- fast, convenient online submission
- thorough peer review by experienced researchers in your field
- rapid publication on acceptance
- support for research data, including large and complex data types
- gold Open Access which fosters wider collaboration and increased citations
- maximum visibility for your research: over 100M website views per year

At BMC, research is always in progress.

Learn more biomedcentral.com/submissions

